Nano Research

Open Access

Research Article

Tailoring pH-ultra-sensitive oncolytic polyesters via a manageable polymer blending strategy

Chanjuan Su[1,§], Yuxuan Zeng[2,3,4,5,§], Shihua Zhang[1,§], Yueling Yuan[1,6,§], Yuxuan Gong[2,3,4,5], Huosheng Zhou[1], Fuxiang Wang[1], Jihong Wang[2,3,4,5] ✉, Menghua Xiong[2,3,4,5] ✉, and Yan Bao[1] ✉

[1] *Guangdong Provincial Key Laboratory of Malignant Tumor Epigenetics and Gene Regulation, Guangdong-Hong Kong Joint Laboratory for RNA Medicine, Medical Research Center, Sun Yat-Sen Memorial Hospital, Sun Yat-Sen University, Guangzhou 510120, China*
[2] *School of Biomedical Sciences and Engineering, South China University of Technology, Guangzhou International Campus, Guangzhou 511442, China*
[3] *National Engineering Research Center for Tissue Restoration and Reconstruction, South China University of Technology, Guangzhou 510006, China*
[4] *Guangdong Province Key Laboratory of Biomedical Engineering, South China University of Technology, Guangzhou 510006, China*
[5] *Key Laboratory of Biomedical Materials of the Ministry of Education, South China University of Technology, Guangzhou 510006, China*
[6] *Guangdong Provincial Key Laboratory of Cancer Pathogenesis and Precision Diagnosis and Treatment, Shenshan Medical Center, Sun Yat-sen Memorial Hospital, Sun Yat-sen University, Shanwei 516621, China*
§ *Chanjuan Su, Yuxuan Zeng, Shihua Zhang, and Yueling Yuan contributed equally to this work.*

Cite this article: *Nano Research*, **2026**, *19*, 94908441. https://doi.org/10.26599/NR.2026.94908441

ABSTRACT: pH-ultra-sensitive oncolytic polymers hold great promise for cancer therapy due to their selective oncolytic activity in the tumor microenvironment. However, achieving well-defined structures and finely tunable pH responsiveness for these polymers remains a challenge. Herein, we developed a straightforward blending strategy using two well-defined alternating polyesters with distinct pH sensitivities to create pH-ultra-sensitive hybrid polyester nanoparticles (Hps) with precisely engineered responsiveness. By varying the mass ratio of the two components, the pK_a of the Hps could be continuously tuned from 6.37 to 7.04. The resulting Hps demonstrated a sharp pH-dependent membranolytic activity switch within a 0.3 pH unit window, with minimal cytotoxicity observed at pH values above the transition pH. A lead Hp formulation identified through screening exhibited potent cytotoxicity at pH 6.8, along with a favorable safety profile and significant antitumor efficacy *in vivo*. This blending strategy establishes a flexible and simple platform for customizing pH responsiveness of oncolytic polymers, advancing oncolytic therapy.

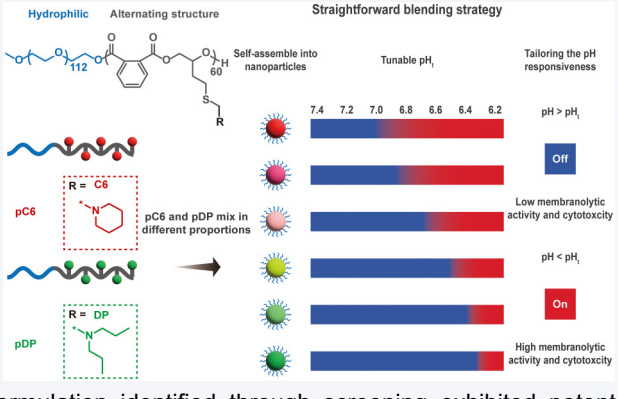

KEYWORDS: pH-ultra-sensitive polymer, oncolytic polymer, pH responsiveness, cancer therapy

1 Introduction

Oncolytic therapy, which directly induces cancer cell death via membrane lysis, holds great potential for cancer therapy [1–4]. This mechanism circumvents the drug resistance and metabolic heterogeneity that critically limit conventional chemotherapy [5–8]. However, the clinical translation of oncolytic agents is severely hampered by their poor selectivity [9–12]. The cationic amphiphilic nature of oncolytic agents, while essential for interacting with negatively charged cancer cell membranes, induces non-specific off-target toxicity toward healthy tissues [13–16]. Designing oncolytic materials that selectively kill tumor cells with minimal toxicity to normal tissue cells is a key challenge, given the subtle differences between tumor and normal tissues/cells.

We and others have developed pH-ultra-sensitive oncolytic polymers (pOPs) capable of switching their membranolytic activity "OFF-to-ON" within a narrow pH window of 0.1–

Received: November 20, 2025; **Revised:** January 10, 2026
Accepted: January 13, 2026

✉Address correspondence to Jihong Wang, wjihong163@163.com; Menghua Xiong, xiongmh@scut.edu.cn; Yan Bao, baoy5@mail.sysu.edu.cn

0.3 units [17–20]. These polymers, functionalized with ionizable tertiary amines and hydrophobic side chains, allow selective activation within the acidic tumor microenvironment (pH 6.5–6.9) while remaining inert in normal tissues (pH 7.2–7.4) [19]. To effectively target the diverse acidic heterogeneity across tumors, it is crucial to finely tune the pH responsiveness of pOPs. Conventional tuning, achieved by adjusting the type and ratio of side-chain groups, relies on extensive chemical screening [21–23]. Moreover, in these random copolymers, a slight (~ 10%) variation in hydrophobic content can shift the pK_a by 0.3–0.4 units, compromising batch-to-batch consistency [18]. Although we recently developed pOPs with a well-defined alternating structure, their pH responsiveness remains constrained by the limited choices for side-chain functionalization [20]. Consequently, developing pOPs that combine a well-defined structure with finely tunable pH responsiveness to match heterogeneous tumor acidity remains a challenge.

We present a straightforward strategy to construct a series of pH-ultra-sensitive hybrid polyester nanoparticles (Hps) with finely tunable responsiveness. We leverage the simple blending of two pH-ultra-sensitive alternating polyesters with distinct pK_a values (7.04 and 6.37). By adjusting the mass ratio of these two polymers, the pK_a of the resulting Hps can be continuously tuned from 6.37 to 7.04, thus precisely controlling the activation transition pH (pH_t) of their oncolytic activity (Fig. 1). The safety profile and antitumor efficacy were then investigated. This blending strategy establishes a flexible and simple platform for customizing oncolytic polymers with distinct pH responsiveness.

2 Results and discussion

2.1 Fine-tuning the pH responsiveness of Hps by simply mixing of two pH-ultra-sensitive polyesters

We synthesized two pH-ultra-sensitive polyesters, mPEG$_{5k}$-(PA-VPO-C6)$_{60}$ (pC6, pK_a = 7.04) and mPEG$_{5k}$-(PA-VPO-DP)$_{60}$ (pDP, pK_a = 6.37) (Fig. 1). They were synthesized through the organocatalytic ring-opening alternating copolymerization of phthalic anhydride (PA) and 3,4-epoxy-1-butene (VPO) by using poly(ethylene glycol) methyl ether (average M_n 5000, mPEG$_{5k}$-OH) as the macroinitiator and phosphazene base (t-BuP1) as the catalyst (Scheme S1, Figs. S1 and S2, and Table S1 in the Electronic Supplementary Material (ESM)) [20, 24, 25]. These polymers were mixed at different mass ratios and dissolved in the organic solvent *N*,*N*-dimethylformamide (DMF), followed by self-assembly into Hps in aqueous solution. We prepared a series of Hps, namely HpC$_3$D$_1$, HpC$_3$D$_2$, HpC$_2$D$_3$, and HpC$_1$D$_3$ (Fig. 1). The letters C and D are abbreviations for pC6 and pDP, respectively, with the subscript indicating the ratio of pC6 to pDP. pH titration experiments revealed that mixing the two polymers allowed for fine-tuning of the pK_a values of the Hps, resulting in pK_a values of 6.87, 6.70, 6.54, and 6.43 (Figs. 2(a) and 2(b)). As the proportion of pDP increased, the pK_a gradually decreased (Fig. 2(b)). Zeta potential characterization demonstrated that the polyesters underwent a charge transition near their pK_a (Fig. S3(a) in the ESM). The particle size was maintained between 10 and 100 nm across a wide pH range, demonstrating adequate stability (Fig. S3(b) in the ESM). This approach enables the simple and controllable construction of oncolytic materials with desired pH responsiveness.

Next, we investigated the pH-dependent membranolytic activity and cytotoxicity of these Hps. *In vitro* cytotoxicity assays revealed that their cytotoxicity was highly pH-dependent (Fig. 2(c)). When the environmental pH exceeded pH_t, minimal cytotoxicity was detected; however, a marked increase in cytotoxicity occurred when the pH dropped below the pH_t (Fig. 2(c)). Panc02$_{GFP/mCherry}$ cells, a pancreatic cancer cell line expressing green fluorescent protein (GFP) on the cell membrane and mCherry in the cytoplasm, were incubated with Hps (200 μg·mL^{-1}) across a range of pH conditions, and the release of cytosolic mCherry was quantified using high-content analysis system (HCAS) (Fig. 2(d)). The results indicated that within a narrow pH window of approximately 0.3 units, the mCherry leakage rate increased sharply from < 10% to

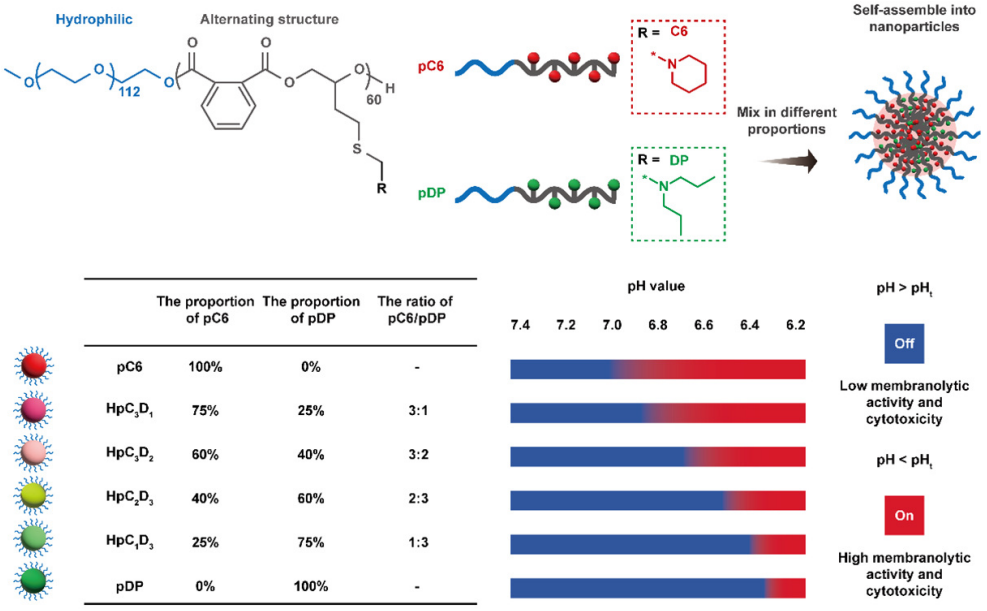

Figure 1 Construction of Hps with finely tunable pH responsiveness by simply mixing two pH-ultra-sensitive polyesters possessing distinct pK_a values. The chemical structures of two pOPs, pC6 and pDP, are shown. Hps were prepared by simply mixing these two polymers in different proportions. Adjusting the ratio of the two pOPs yielded Hps with tunable pH responsiveness. These Hps show low membranolytic activity and cytotoxicity at pH > pH_t, while exhibiting potent effects at pH < pH_t.

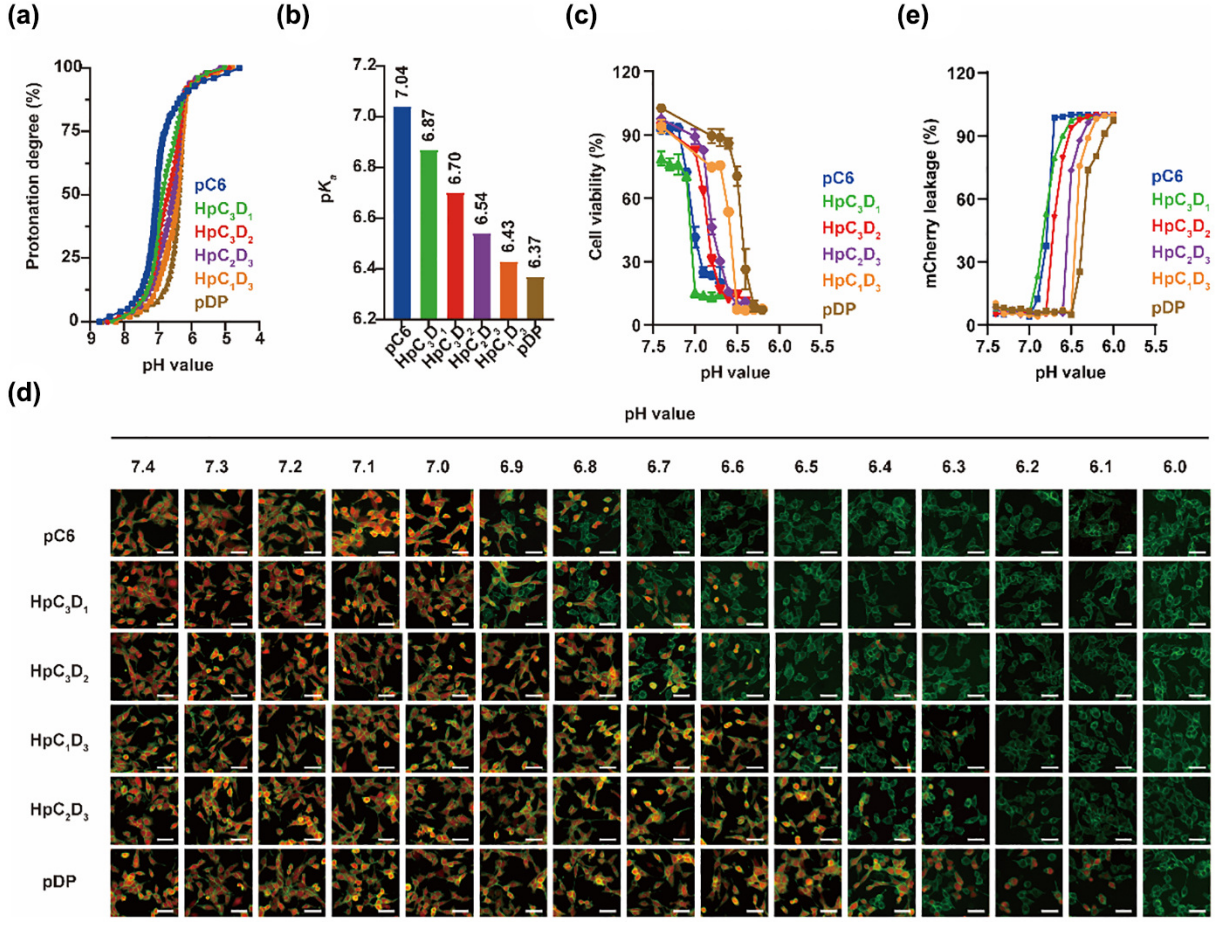

Figure 2 Tunable pH-responsive membranolytic activity of Hps. (a) Protonation degree as a function of pH for Hps. (b) The pK_a values of the Hps determined from titration curves. (c) The cell viability of Hps (400 μg·mL^{-1}) against Panc02 cells under different pH conditions after 4 h incubation. (d) Representative HCAS images of Panc02$_{GFP/mCherry}$ cells treated with Hps (200 μg·mL^{-1}) for 4 h at indicated pH values. The red fluorescence represents the fluorescent protein mCherry while the green fluorescence represents the fluorescent protein MyrPalm-GFP. Scale bars: 40 μm. (e) Quantification of mCherry leakage following 4 h incubation with Hps against Panc02 $_{GFP/mCherry}$ cells at pH 6.8. In (c), n = 3 biologically independent samples were tested, and data are presented as mean ± standard deviation (SD). In (e), n = 9 fields of vision were selected for the analysis.

> 80% (Fig. 2(e)). Collectively, these results indicated that these Hps exhibited sharp, pH-dependent membranolytic activity.

2.2 Phosphatidylserine contributes to the membranolytic activity

Using HpC_3D_2 as a representative formulation, we next sought to elucidate its mechanism of pH-responsive cytotoxicity. Liposome dye leakage assays demonstrated that the membranolytic activity of HpC_3D_2 increased as pH decreased (Fig. 3(a)). At pH 6.8, HpC_3D_2 induced concentration-dependent release of adenosine triphosphate (ATP) (Fig. 3(b)), lactate dehydrogenase (LDH) (Fig. 3(c)), and intracellular proteins (Fig. 3(d)), whereas no such release was observed at pH 7.4 (Figs. 3(b)–3(d)). Time-lapse imaging via spinning disk confocal microscopy further revealed that treatment with HpC_3D_2 caused rapid rupture of plasma membrane, accompanied by release of intracellular mCherry within 30 min (Fig. 3(e) and Videos S1 and S2 in the ESM). *In vitro* cytotoxicity assays revealed that HpC_3D_2 exhibited similar cytotoxic effects against various tumor cell lines at pH 6.8 (Fig. S4(a) in the ESM). In contrast, no significant cytotoxicity was observed at physiological pH 7.4 (Fig. S4(b) in the ESM). Moreover, the cytotoxic effect of HpC_3D_2 at pH 6.8 was not inhibited by endocytosis inhibitors (Fig. S5(a) in the ESM), cell death pathway inhibitors (Fig. S5(b) in the ESM), or variations in temperature (Fig. S5(c) in the ESM).

Given that tumor-cell membranes are enriched in anionic phospholipids—especially phosphatidylserine (PS) [26–28], we investigated whether PS affects the membranolytic activity of HpC_3D_2. We performed cytotoxicity assay against Panc02 at pH 6.8. In the presence of PS (640 μg·mL^{-1}), the cytotoxicity of HpC_3D_2 against Panc02 cells was significantly suppressed (Fig. 3(f)). Next, we performed isothermal titration calorimetry (ITC) to evaluate the binding of HpC_3D_2 to phospholipids. A strong interaction was detected between HpC_3D_2 and PS at pH 6.8, with a binding constant (K_a) of 3.66 × 10^5 M^{-1} (Figs. 3(g) and 3(h), and Table S2 in the ESM). In contrast, no obvious binding was observed with phosphatidylcholine (PC) or phosphatidylethanolamine (PE) (Figs. 3(g) and 3(h)). Moreover, Annexin V-fluorescein isothiocyanate (FITC) labeling demonstrated that the exposure of externalized PS on the cell surface increased in a time-dependent manner (Fig. 3(i) and Video S3 in the ESM). In parallel, the number of propidium-iodide (PI)-positive cells also increased (Fig. 3(i) and Video S3 in the ESM). Collectively, these results indicate that, under acidic conditions, HpC_3D_2 induces PS-dependent membrane permeabilization, intracellular-component leakage, and ultimately tumor-cell death.

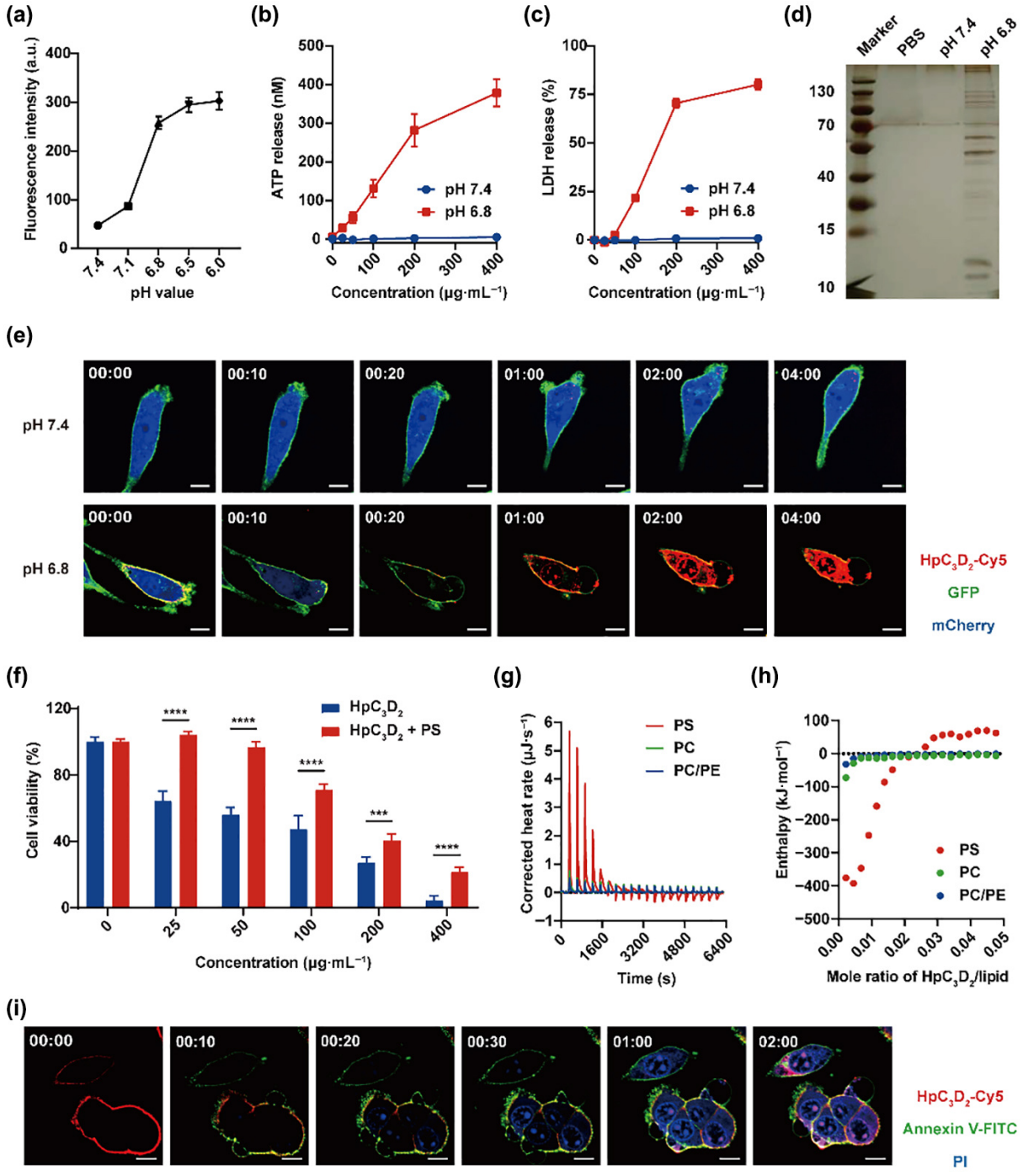

Figure 3 PS contributes to the cytotoxic effect of HpC_3D_2. (a) Dye leakage from cancer cell membrane-mimicking liposomes treated with HpC_3D_2 (200 μg·mL^{-1}) for 10 min under varying pH conditions. (b) ATP and (c) LDH release from Panc02 cells treated with HpC_3D_2 at different concentrations under pH 7.4 or 6.8. (d) SDS-polyacrylamide gel electrophoresis (SDS-PAGE) analysis of intracellular protein release into supernatant after treatment with HpC_3D_2 (200 μg·mL^{-1}) at pH 7.4 or 6.8. (e) Spinning disk confocal images of $Panc02_{GFP/mCherry}$ cells after 4 h treatment with HpC_3D_2 (200 μg·mL^{-1}) at pH 7.4 and pH 6.8. HpC_3D_2-Cy5, in red; MyrPalm-GFP, in green; and mCherry, in blue. Scale bars: 10 μm. (f) Cytotoxicity of HpC_3D_2 against Panc02 cells at pH 6.8 in the presence of PS (640 μg·mL^{-1}). (g) ITC profile of the binding between HpC_3D_2 and PS, PC and PE at pH 6.8. (h) Integrated heat changes derived from the titration of HpC_3D_2 with PS, PC and PE at pH 6.8. (i) Fluorescence microscopy images of Panc02 cells treated with HpC_3D_2-Cy5 and co-stained with Annexin V-FITC and PI over time at pH 6.8. Scale bars: 10 μm. In (a)–(c) and (f), $n = 3$ biologically independent samples were tested, and data are presented as mean ± SD. Statistical significance was determined by unpaired two-tailed Student's t-test; $^{***}P < 0.001$, $^{****}P < 0.0001$.

2.3 *In vivo* toxicity profile and anti-tumor efficacy of Hps

An *in vivo* toxicity assessment was performed. We determined the maximum tolerated dose (MTD) of Hps against ICR (Institute of Cancer Research) mice upon intravenous administration. The MTD increased as the pK_a decreased: pC6 and HpC_3D_1 (highest pK_a) showed an MTD of 100 mg·kg^{-1}; HpC_3D_2, HpC_2D_3, and HpC_1D_3 (moderate pK_a) showed 150 mg·kg^{-1}; and pDP (lowest pK_a) exceeded 200 mg·kg^{-1} (Fig. 4(a)). At a dose of 50 mg·kg^{-1},

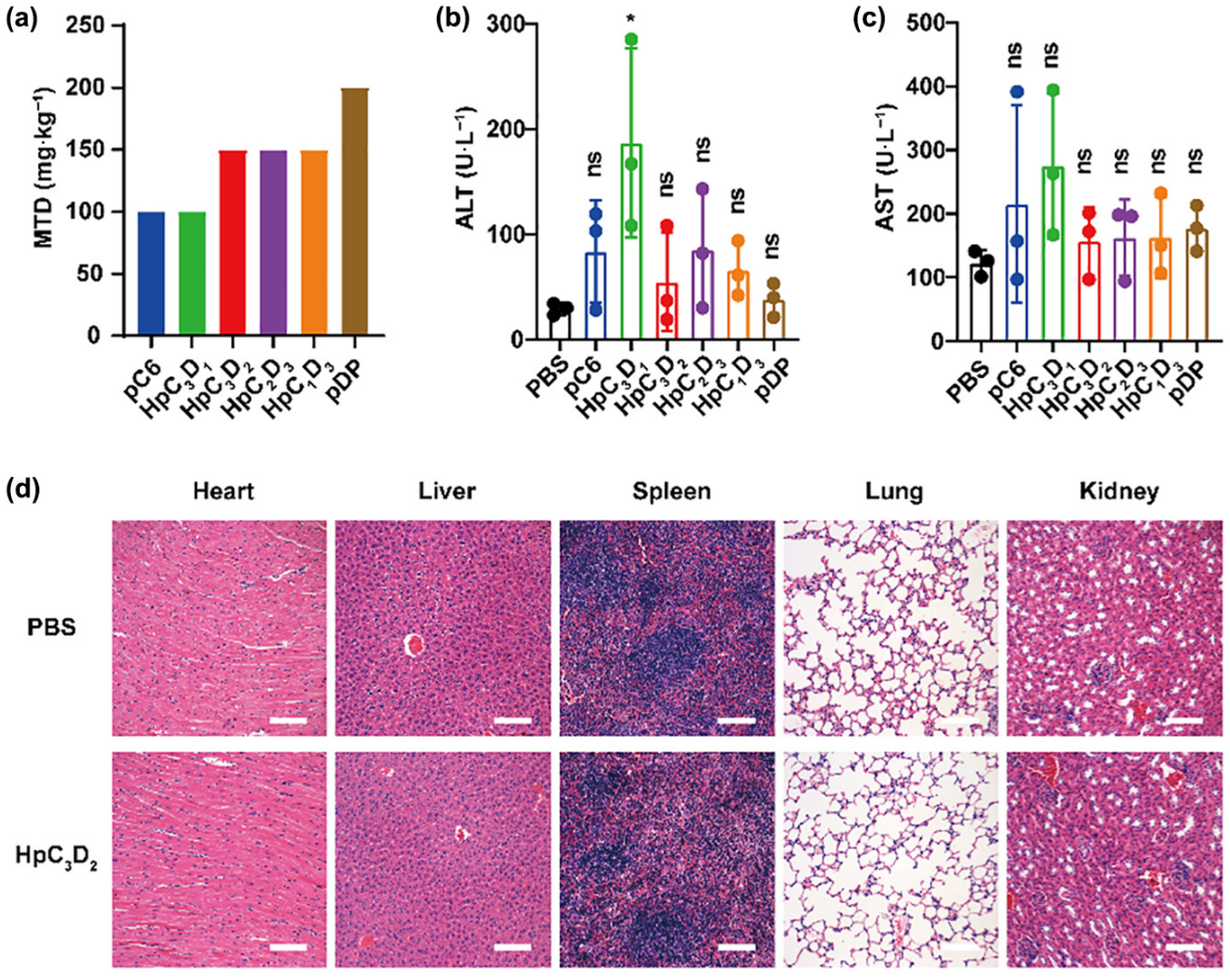

Figure 4 The *in vivo* toxicity of the Hps. (a) The MTD of Hps against ICR mice after intravenous administration at a dose of 50 mg·kg^{-1}. The concentrations of (b) ALT and (c) AST in the serum 24 h after one intravenous injection of Hps into ICR mice at a dose of 50 mg·kg^{-1} (n = 3 per group) and data are presented as mean ± SD. (d) H&E staining of major organs collected 24 h after one dose of HpC_3D_2 (50 mg·kg^{-1}). Scale bars: 50 μm. Representative images from at least three independent mice are shown. Statistical significance was determined by Dunn's multiple comparisons test, * $P < 0.05$, ns indicates no significance.

intravenous administration of most Hps did not induce significant elevation of liver enzymes (alanine transaminase (ALT), aspartate transferase (AST), urea, or uric acid (UA)) in serum of ICR mice, with the exception of HpC_3D_1 (Figs. 4(b) and 4(c) and Fig. S6 in the ESM). Hematoxylin-eosin (H&E) staining of major organs revealed no obvious histological abnormalities (Fig. 4(d) and Fig. S7 in the ESM).

Then, we evaluated the *in vivo* therapeutic efficacies of four Hps with MTD exceeding 150 mg·kg^{-1} in the Panc02 model. Among them, HpC_3D_2 exhibited the most potent antitumor efficacy (Figs. 5(a)–5(d)). In the MC38 model, treatment with HpC_3D_2 also significantly suppressed tumor growth compared to the control group, as evidenced by reduced tumor volumes and representative tumor images (Figs. 5(e)–5(h)). Significant therapeutic effects were also detected in the 4T1 (Figs. 5(i)–5(l)) and EO771 (Figs. 5(m)–5(p)) tumor models. Notably, in the EO771 model, complete tumor regression was observed in three out of five mice. In addition, HpC_3D_2 administration did not cause significant body weight loss (Fig. S8 in the ESM). Histological analysis by H&E staining revealed focal necrosis in HpC_3D_2-treated tumors (Fig. 5(q)). Characteristic morphological alterations—including nuclear pyknosis, karyorrhexis, loss of cellular architecture, and indistinct cell boundaries—were observed (Fig. 5(q)), suggesting that HpC_3D_2 effectively targets tumor cells and induces membrane disruption and cellular damage.

Finally, we examined the tissue distribution and pharmacokinetics of HpC_3D_2 following intravenous injection. HpC_3D_2 was detected in the liver, spleen, lungs, kidneys, and tumors within 24 h, with the highest accumulation found in the liver (Figs. S9(a) and S10(b) in the ESM). Pharmacokinetic analysis revealed rapid clearance from the bloodstream, with an elimination half-life of 0.20 h (Fig. S9(c) in the ESM).

3 Conclusions

Overall, we developed a straightforward and effective strategy to precisely adjust the pH responsiveness of pH-ultra-sensitive oncolytic polyesters by simply blending two alternating polyesters with different pH sensitivities. Our blending method offers a flexible platform for tailoring pH-responsiveness of oncolytic polymers.

Electronic Supplementary Material: Supplementary material (experimental methods; Scheme S1: Schematic illustration of the synthetic route of pC6 or pDP; Scheme S2: Schematic illustration of

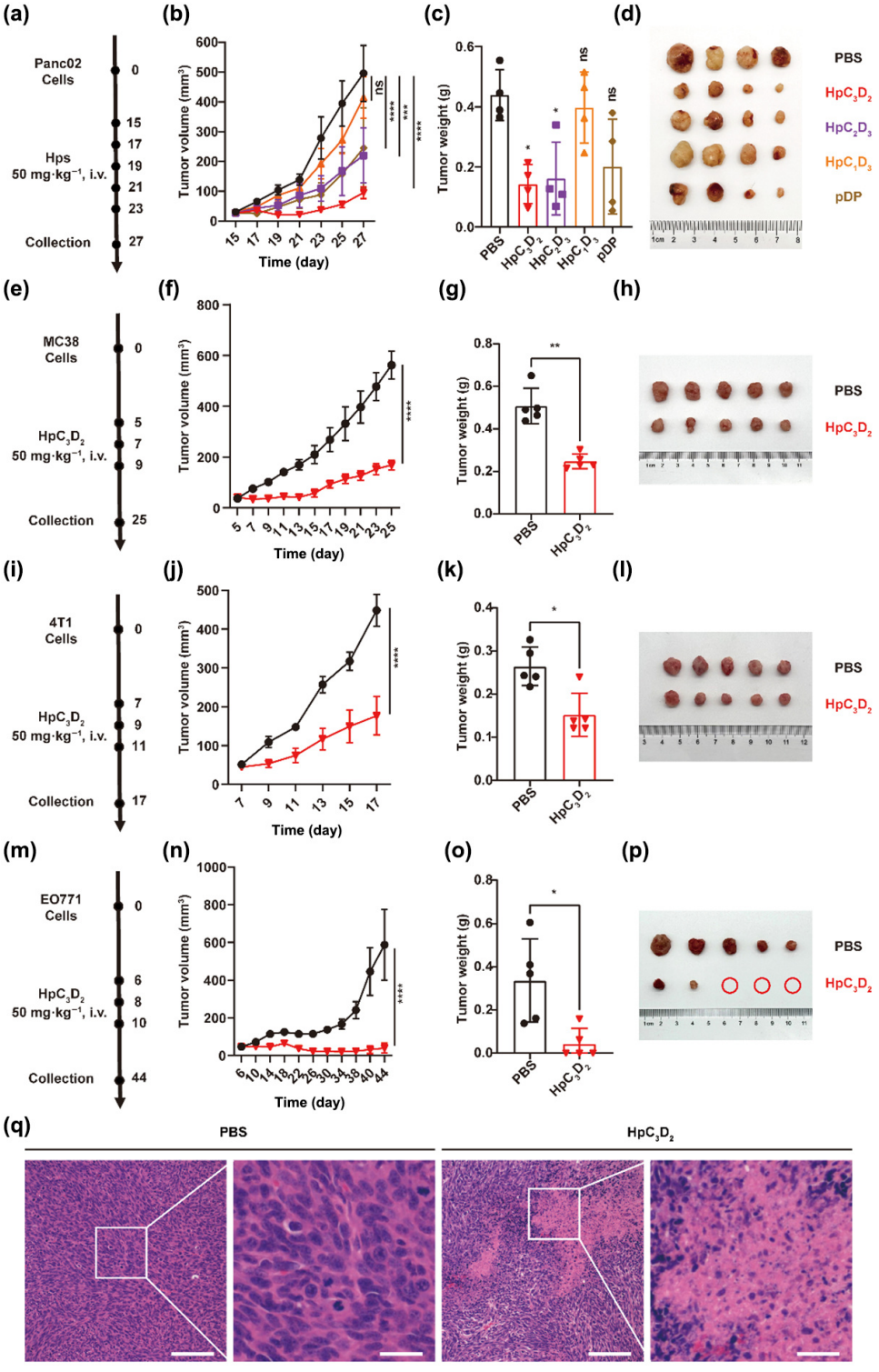

Figure 5 HpC_3D_2 exhibits potent antitumor efficacy *in vivo*. (a) Treatment schedule for Panc02 tumor model (n = 4 per group). C57BL/6 mice were inoculated with Panc02 cells on day 0. Tumor-bearing mice were then treated with Hps (50 mg·kg^{-1}) from days 15 to 23 every other day. (b) Tumor growth curves of Panc02-bearing mice. (c) Tumor weight and (d) tumor images of excised Panc02 tumors at the endpoint. (e) Treatment schedule for MC38 tumor model (n = 5 per group). C57BL/6 mice were inoculated with MC38 cells on day 0, followed by administration of HpC_3D_2 (50 mg·kg^{-1}) from days 5 to 9 every other day. (f) Tumor growth curves of MC38-bearing mice. (g) Tumor weights and (h) tumor images of excised MC38 tumors at the endpoint. (i) Treatment schedule for 4T1 tumor model (n = 5 per group). BALB/c mice were inoculated with 4T1 cells on day 0 and treated with HpC_3D_2 (50 mg·kg^{-1}) every other day from days 7 to 11. (j) Tumor growth curves of 4T1-bearing mice. (k) Tumor weights and (l) photographs of excised 4T1 tumors. (m) Treatment schedule for the EO771 tumor model (n = 5 per group). C57BL/6 mice were inoculated with EO771 cells on day 0 and treated with HpC_3D_2 (50 mg·kg^{-1}) every other day from days 6 to 10. (n) Tumor growth curves of EO771-bearing mice. (o) Tumor weights and (p) photographs of excised EO771 tumors. (q) H&E staining of MC38 tumor tissues collected at the endpoint. Scale bars: 100 μm (overview) and 25 μm (magnified view). Data are presented as mean ± standard error of mean (SEM). Statistical significance was determined by unpaired Mann-Whitney U test for tumor weight; tumor volume data were analyzed by two-way ANOVA. *P < 0.05, **P < 0.01, ***P < 0.001, ****P < 0.0001, ns indicates no significance.

the synthetic route of polyester-Cy5; Figure S1: ^{1}H nuclear magnetic resonance (NMR) spectra (400 MHz) of pC6, pDP, and P(P-V); Figure S2: ^{13}C NMR spectrum of P(P-V); Figure S3: The zeta potential and size of Hps; Figure S4: Concentration-dependent cytotoxicity of HpC_3D_2 against multiple cancer cell lines; Figure S5: Cytotoxicity of HpC_3D_2 against Panc02 cells at pH 6.8 after 4 h pretreatment with various conditions; Figure S6: The concentrations of (a) Urea and (b) UA in the serum 24 h after one intravenous injection of Hps into ICR mice at a dose of 50 mg·kg^{-1} (n = 3 per group); Figure S7: H&E staining of Panc02 tumor tissues; Figure S8: The weight of mice during treatments of Panc02 tumors; Figure S9: The pharmacokinetic behaviors and distribution of HpC_3D_2; Table S1: Characterization of polyesters; Table S2: Thermodynamic parameters for interaction of HpC_3D_2 with PS obtained from ITC at pH 6.8) is available in the online version of this article at https://doi.org/10.26599/NR.2026.94908441.

Data availability

All data needed to support the conclusions in the paper are presented in the manuscript and the Electronic Supplementary Material. Additional data related to this paper may be requested from the corresponding author upon request.

Acknowledgements

This work was supported by the National Natural Science Foundation of China (Nos. 32522050, 32371389, and 52273127), Guangdong Basic and Applied Basic Research Foundation (Nos. 2023B1515020086, and 2023A1515111158), Guangdong Science and Technology Department (No. 2024B1212030002), and Guangdong Provincial Medical Research Fund (No. B2025269).

Declaration of competing interest

All the contributing authors report no conflict of interests in this work.

Author contribution statement

C. J. S.: Writing – original draft, software, methodology, investigation, conceptualization. Y. X. Z.: Writing – review & editing, investigation. S. H. Z.: Writing – review & editing, investigation. Y. L. Y.: Writing – review & editing, validation, visualization. Y. X. G.: Investigation. H. S. Z.: Investigation. F. X. W.: Investigation. J. H. W.: Writing – review & editing, supervision, validation, visualization. M. H. X.: Writing – review & editing, supervision, resources, funding acquisition, data curation, conceptualization. Y. B.: Writing – review & editing, supervision, resources, funding acquisition, data curation, conceptualization.

Informed consent

Not applicable.

Ethics statement

The animal experiments were carried out following the guidelines of the South China University of Technology Animal Care and Use Committee (AE-2025080).

Use of AI statement

None.

References

[1] Ribas, A.; Dummer, R.; Puzanov, I.; VanderWalde, A.; Andtbacka, R. H. I.; Michielin, O.; Olszanski, A. J.; Malvehy, J.; Cebon, J.; Fernandez, E. et al. Oncolytic virotherapy promotes intratumoral T cell infiltration and improves anti-PD-1 immunotherapy. *Cell.* **2017**, *170*, 1109–1119.e10.

[2] Lin, D. N.; Shen, Y. N.; Liang, T. B. Oncolytic virotherapy: Basic principles, recent advances and future directions. *Sig. Transduct. Target. Ther.* **2023**, *8*, 156.

[3] Twumasi-Boateng, K.; Pettigrew, J. L.; Kwok, Y. Y. E.; Bell, J. C.; Nelson, B. H. Oncolytic viruses as engineering platforms for combination immunotherapy. *Nat. Rev. Cancer.* **2018**, *18*, 419–432.

[4] Liu, H. M.; Shen, W.; Liu, W. G.; Yang, Z. X.; Yin, D. K.; Xiao, C. S. From oncolytic peptides to oncolytic polymers: A new paradigm for oncotherapy. *Bioact. Mater.* **2024**, *31*, 206–230.

[5] Shao, N.; Yuan, L.; Liu, L. Q.; Cong, Z. H.; Wang, J. Z.; Wu, Y. M.; Liu, R. H. Reversing anticancer drug resistance by synergistic combination of chemotherapeutics and membranolytic antitumor β-peptide polymer. *J. Am. Chem. Soc.* **2024**, *146*, 11254–11265.

[6] Dai, W. W.; Tian, R. T.; Yu, L. B.; Bian, S. S.; Chen, Y. L.; Yin, B. W.; Luan, Y. X.; Chen, S. Q.; Fan, Z. Y.; Yan, R. C. et al. Overcoming therapeutic resistance in oncolytic herpes virotherapy by targeting IGF2BP3-induced NETosis in malignant glioma. *Nat. Commun.* **2024**, *15*, 131.

[7] Wu, H. Y.; Zhong, D.; Zhang, Z. J.; Li, Y. C.; Zhang, X.; Li, Y. K.; Zhang, Z. Z.; Xu, X. H.; Yang, J.; Gu, Z. W. Bioinspired artificial tobacco mosaic virus with combined oncolytic properties to completely destroy multidrug-resistant cancer. *Adv. Mater.* **2020**, *32*, 1904958.

[8] Yang, J.; Zheng, R.; Mamuti, M.; Hou, D. Y.; Zhao, Y. D.; An, H. W.; Wang, H.; Zhao, Y. L. Oncolytic peptide nanomachine circumvents chemo resistance of renal cell carcinoma. *Biomaterials* **2022**, *284*, 121488.

[9] Hilchie, A. L.; Hoskin, D. W.; Power Coombs, M. R. Anticancer activities of natural and synthetic peptides. *Adv. Exp. Med. Biol.* **2019**, *1117*, 131–147.

[10] Shalhout, S. Z.; Miller, D. M.; Emerick, K. S.; Kaufman, H. L. Therapy with oncolytic viruses: Progress and challenges. *Nat. Rev. Clin. Oncol.* **2023**, *20*, 160–177.

[11] Aghamiri, S.; Zandsalimi, F.; Raee, P.; Abdollahifar, M. A.; Tan, S. C.; Low, T. Y.; Najafi, S.; Ashrafizadeh, M.; Zarrabi, A.; Ghanbarian, H. et al. Antimicrobial peptides as potential therapeutics for breast cancer. *Pharmacol. Res.* **2021**, *171*, 105777.

[12] Appleton, E.; Chiocca, E. A.; Ungerechts, G.; Melcher, A.; Vile, R. Oncolytic viruses as anticancer agents: Clinical progress and remaining challenges. *Lancet* **2025**, *406*, 1295–1312.

[13] Palermo, E. F.; Lienkamp, K.; Gillies, E. R.; Ragogna, P. J. Antibacterial activity of polymers: Discussions on the nature of amphiphilic balance. *Angew. Chem., Int. Ed.* **2019**, *58*, 3690–3693.

[14] Quemé-Peña, M.; Juhász, T.; Kohut, G.; Ricci, M.; Singh, P.; Szigyártó, I. C.; Papp, Z. I.; Fülöp, L.; Beke-Somfai, T. Membrane association modes of natural anticancer peptides: Mechanistic details on helicity, orientation, and surface coverage. *Int. J. Mol. Sci.* **2021**, *22*, 8613.

[15] Zhong, C.Y.; Li, J.; Liu, S. P.; Li, W. R.; Zhang, Q.; Zhao, J. P.; Xiong, M. H.; Bao, Y.; Yao, Y. D. Nanoblock-mediated selective oncolytic polypeptide therapy for triple-negative breast cancer. *Theranostics* **2023**, *13*, 2800–2810.

[16] Tornesello, A. L.; Borrelli, A.; Buonaguro, L.; Buonaguro, F. M.; Tornesello, M. L. Antimicrobial peptides as anticancer agents: Functional properties and biological activities. *Molecules* **2020**, *25*, 2850.

[17] Bennett, Z. T.; Huang, G.; Dellinger, M. T.; Sumer, B. D.; Gao, J. M. Stepwise ultra-pH-sensitive micelles overcome a pK_a barrier for systemic lymph node delivery. *ACS Nano* **2024**, *18*, 16632–16647.

[18] Zhang, W. N.; Wang, X. C.; Wang, J. H.; Su, C. J.; Bao, Y.; Xiong, M. H. The relationship between *in vivo* toxicity and responsive pH in transistor-like pH-sensitive nanodetergents. *Small Methods* **2025**, *9*, 2401263.

[19] Liu, M. D.; Huang, L. Q.; Zhang, W. N.; Wang, X. C.; Geng, Y. Y.; Zhang, Y. H.; Wang, L.; Zhang, W. B.; Zhang, Y. J.; Xiao, S. Y. et al. A transistor-like pH-sensitive nanodetergent for selective cancer therapy. *Nat. Nanotechnol.* **2022**, *17*, 541–551.

[20] Wang, J. H.; Yuan, Y. L.; Su, C. J.; Bao, Y.; Xu, W. D.; Yao, Y. D.; Liang, L. F.; Zeng, Y. X.; Xiong, M. H. pH-ultrasensitive membranolytic polyesters with alternating sequence of ionizable and hydrophobic groups for selective oncolytic therapy. *J. Am. Chem. Soc.* **2025**, *147*, 1008–1016.

[21] Tay, J.; Zhao, Y. L.; Hedrick, J. L.; Yang, Y. Y. Elucidating the anticancer activities of guanidinium-functionalized amphiphilic random copolymers by varying the structure and composition in the hydrophobic monomer. *Theranostics* **2021**, *11*, 8977–8992.

[22] Palermo, E. F.; Vemparala, S.; Kuroda, K. Cationic spacer arm design strategy for control of antimicrobial activity and conformation of amphiphilic methacrylate random copolymers. *Biomacromolecules* **2012**, *13*, 1632–1641.

[23] Chen, Y. F.; Shiau, A. L.; Chang, S. J.; Fan, N. S.; Wang, C. T.; Wu, C. L.; Jan, J. S. One-dimensional poly(L-lysine)-*block*-poly(L-threonine) assemblies exhibit potent anticancer activity by enhancing membranolysis. *Acta Biomater.* **2017**, *55*, 283–295.

[24] Li, H.; Zhao, J. P.; Zhang, G. Z. Self-buffering organocatalysis tailoring alternating polyester. *ACS Macro Lett.* **2017**, *6*, 1094–1098.

[25] Hao, J.; Kos, P.; Zhou, K. J.; Miller, J. B.; Xue, L.; Yan, Y. F.; Xiong, H.; Elkassih, S.; Siegwart, D. J. Rapid synthesis of a lipocationic polyester library via ring-opening polymerization of functional valerolactones for efficacious siRNA delivery. *J. Am. Chem. Soc.* **2015**, *137*, 9206–9209.

[26] Burstyn-Cohen, T.; Maimon, A. TAM receptors, phosphatidylserine, inflammation, and cancer. *Cell Commun. Signal.* **2019**, *17*, 156.

[27] Wang, W. H.; Wu, S. X.; Cen, Z. P.; Zhang, Y. X.; Chen, Y. A.; Huang, Y. X.; Cillo, A. R.; Prokopec, J. S.; Quarato, G.; Vignali, D. A. A. et al. Mobilizing phospholipids on tumor plasma membrane implicates phosphatidylserine externalization blockade for cancer immunotherapy. *Cell Rep.* **2022**, *41*, 111582.

[28] Wu, M. H.; Shi, P. S.; Huang, J. M.; Ni, X. M.; Lai, R. J.; Cao, K.; Cai, M. Y.; Yu, H.; Zhao, W. S.; Zhang, Y. TMEM16F phospholipid scramblase regulates tumorigenesis by modulating the tumor immune microenvironment. *Proc. Natl. Acad. Sci. USA* **2025**, *122*, e2513910122